

Refining the CLARREO Mission by Correlating Ozone and Temperature Profiles with Cross-track Infrared Sounder (CrIS) Infrared Brightness Temperature Spectra

Ester Nikolla, Robert Knuteson, Michelle Feltz, and Henry Revercomb

University of Wisconsin-Madison Space Science and Engineering Center (SSEC)
Cooperative Institute for Meteorological Satellite Studies (CIMSS)

1. INTRODUCTION

Global carbon dioxide (CO₂) concentrations have been steadily increasing for the last 50 years as illustrated in Figure 1. The increase in global CO₂ concentration has been predicted to cause a cooling effect in the stratosphere due to increased infrared radiative emission to space from the 15 μm absorption band of CO₂ (Ramaswamy et al. 2001). The CO₂ molecule has the four vibrational modes shown in Figure 2.

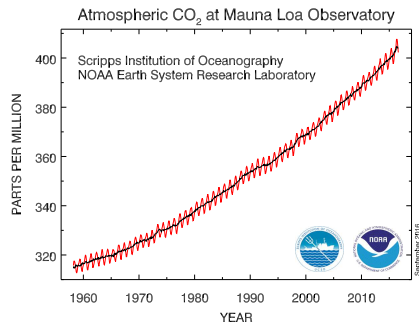


Figure 1. Increasing carbon dioxide levels as measured by NOAA at Mauna Loa, Hawaii.
<http://www.esrl.noaa.gov/gmd/ccgg/trends>

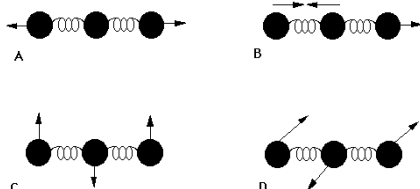


Figure 2. Illustration of the four vibration modes of the linear molecule CO₂; mode A does not have an IR absorption, stretching mode B absorbs at 2349 cm⁻¹, bending modes C and D absorb at 667 cm⁻¹ (15 μm).
<http://wag.caltech.edu/home/jang/genchem/infrared.htm>

Ozone (O₃) is a triatomic molecule and a powerful oxidizing agent. The formation of ozone in the stratosphere is initiated by ultraviolet (UV) sunlight and results in the reaction of molecular oxygen (O₂) and atomic oxygen (O) in the presence of a third body, e.g. nitrogen. Without this absorption, the combining of O and O₂ into ozone cannot be completed. Figure 3 illustrates the creation of stratospheric ozone caused by sunlight incident on the top of the atmosphere.

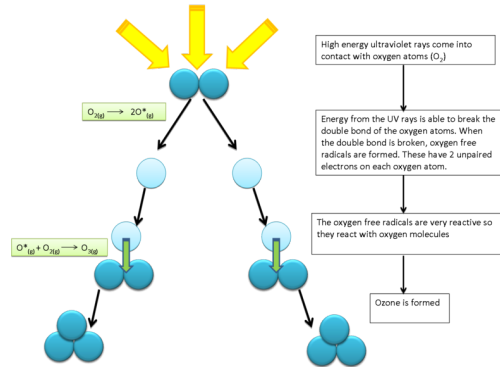


Figure 3. Ozone creation in the stratosphere.
<http://envirochemsa.wikispaces.com>

The vertical profile shown in Figure 4 indicates how ozone amount varies with height in the atmosphere. Note that most of the ozone is in the lower stratosphere. The "ozone layer" resides at an altitude of about 20 to 25 kilometers above sea level. The ozone layer blocks the sun's UV-B radiation which has harmful effects on plants and animals. The chlorine and bromine in human-produced chemicals such as the ones known as chlorofluorocarbons (CFCs) and halons can deplete ozone in the stratosphere. Figure 4 shows a simplified cycle of reactions in which UV light breaks up CFCs and the resulting chlorine (Cl) atom destroys ozone (O₃) molecules. Ozone levels decreased from the 1970s through the 1990s, most obviously in the polar regions. (<http://www.ozonelayer.noaa.gov/science/o3depletion.htm>)

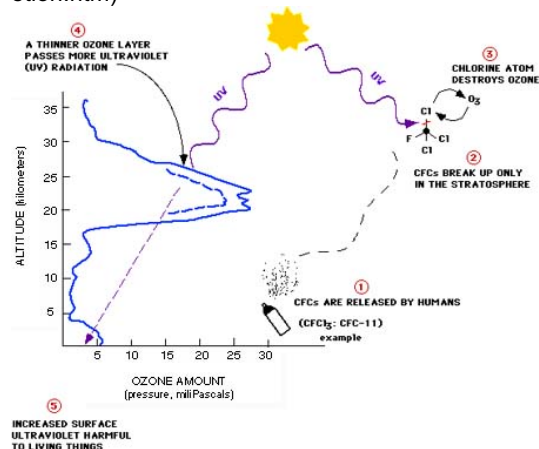


Figure 4. Illustration of ozone destruction in the stratosphere by chlorine atoms carried aloft by CFC.
<http://www.ozonelayer.noaa.gov>

The Montreal Protocol on Substances that Deplete the Ozone Layer enacted in 1987, banned the production of CFCs. The stratospheric ozone levels are expected to recover over the next 50 years. This increase in ozone concentration is expected to contribute a warming effect in the stratosphere, which is expected to compensate for the cooling effect of increasing carbon dioxide concentrations in the stratosphere (Seidel et al. 2016; Maycock 2016).

The detection of temperature trends in the stratosphere has proven challenging due to lack of well-calibrated measurements from in situ (weather balloon borne radiosondes) and satellite passive IR and microwave sensors. (Randel et al. 2009). The recent record of radio occultation (RO) measurements from space provides a new set of global temperature observations but with significant sampling only since 2007 (Steiner et al. 2013, 2011; Ho et al. 2010). Another recent development is the use of accurate spectrally resolved infrared radiance to investigate trends in infrared brightness temperature (Huang and Ramaswamy 2009, Tobin et al. 2013, Pan et al. 2015). Initial comparisons between RO and IR observations indicate that the lower stratosphere is a region where both measurements have shown good agreement of approximately a few tenths of a degree Celsius (Feltz et al. 2014). The use of SI traceable measurements from space in the measurement of climate temperature trends is the goal of the CLARREO mission (Wielicki et al. 2013). The time to detect trends is a combination of the natural variability and measurement error plus any autocorrelation of the time series.

The objective of this study is to investigate the correlation of the infrared brightness temperature spectra from Earth orbiting satellites with time and space coincident vertical profiles of atmospheric ozone concentration. Ozone vertical profiles are computed in ten-degree latitude zones along with corresponding infrared brightness temperature mean spectra.

2. DATA

The data used in this study are from the Cross-track InfraRed Sounder (CrIS) and the Ozone Mapping Profiler Suite (OMPS) on the NASA Suomi-NPP satellite platform. Figure 5 shows the CrIS and OMPS on the nadir viewing deck of the Suomi-NPP satellite. The Suomi-NPP satellite is in a sun-synchronous polar orbit with a 1:30 pm equator crossing time, similar to the NASA Aqua satellite but at a higher altitude. The Suomi-NPP satellite has an instrument suite which closely matches that of the operational Joint Polar Satellite System (JPSS) expected to be launched in early 2017.

The Cross-track Infrared Sounder (CrIS), provides soundings of the atmosphere with 1305 spectral channels, over 3 wavelength ranges: LW (9.14 - 15.38 μ m); MW (5.71 - 8.26 μ m); and SW (3.92 - 4.64 μ m). The longwave band resolution is 0.625 cm^{-1} . The CrIS instrument is a Fourier transform spectrometer which records the interference pattern of the infrared wavelengths which are contained in each of the LW, MW, and SW spectral bands. As the satellite orbits from pole to pole, the CrIS sensor uses a 45 degree mirror to scan a 2200km swath width (\pm 50 degrees), with 30 Earth-scene fields of regard. Each field of regard consists of 9 fields of view, arrayed as 3x3 array of 14km diameter spots (at nadir). This yields 90 Earth views across track. Each scanline includes views of the internal calibration target (warm calibration point), and a deep space view (cold calibration point). The CrIS sensor on Suomi-NPP has demonstrated excellent absolute accuracy (Tobin et al. 2013).



Figure 5. Photo image of the NASA Suomi-NPP satellite with labels for the five sensors. (<https://jointmission.gsfc.nasa.gov/cris.html>)

The raw CrIS interferogram packets used in this study were obtained from the NOAA CLASS archive (<http://www.class.ncdc.noaa.gov>). In order to create a consistent radiance record, the CrIS radiance spectra were reprocessed at the University of Wisconsin-Madison Space Science and Engineering Center (SSEC) using JPSS software available for use with direct broadcast. (http://cimss.ssec.wisc.edu/cspp/npp_sdr_v2.2.3.shtml).

Vertical profiles of ozone concentration along the nadir satellite track of Suomi-NPP were obtained from the NASA OMPS science team archive at <https://ozoneaq.gsfc.nasa.gov/data/omps/>. An example OMPS daily product data file is named OMPS-NPP_LP-L2-O3-DAILY_v2.3_...h5. The spectral measurements from the OMPS Nadir Profiler and Nadir Mapper of the solar radiances scattered by the Earth's atmosphere are used to generate estimates of the ozone vertical profile along the orbital track. Eight channels from the Nadir Profiler and four from the Nadir Mapper are used to obtain estimates of the total column ozone, effective reflectivity, and the ozone vertical profile in 12 layers. For the combined ozone density profile used here, the VIS retrieval results are used between 0-26.5 km, and the UV retrieval results are used between 27.5-60.5 km. (http://ozoneaq.gsfc.nasa.gov/omps/media/docs/LP-L2-O3-DAILY_V2_Product_Description.pdf)

3. METHODOLOGY

The CrIS radiance spectra near nadir were extracted from the CrIS cross-track scanlines for each UTC day. The two CrIS fields of view that bracket the satellite nadir track (element 45 and 46 out of 90) were selected. A daily nadir CrIS radiance file was created that contained all three CrIS spectral bands for each day from 1 April 2012 through 31 March 2016. A set of zonal mean radiance spectra were computed for each day of the three-year period using 10-degree latitude bins. The CrIS zonal brightness temperature spectra used in this study contain the average of both sunlit and nighttime portions of the latitude zone. The zonal mean radiances were converted to brightness temperature spectra using a Planck curve at the scene radiance to find the equivalent blackbody temperature. A global mean radiance was computed by weighting each latitude zone average radiance spectrum by the cosine of the mean latitude. This is equivalent to an area weighted average. The corresponding global mean brightness temperature was computed from the global mean radiance spectrum for each day.

The natural variability of the infrared brightness temperature is defined to be the inter-annual

variability computed from annual means. A global three-year mean CrIS brightness temperature was computed from the global daily mean CrIS brightness temperature spectra. The annual mean CrIS brightness temperature was computed for the calendar years 2013, 2014, and 2015. The deviation from the mean and the standard deviation (inter-annual variability) are computed for each CrIS spectral channel.

Two CrIS brightness temperature (BT) spectral channels were selected which peak in the upper stratosphere (667.5 cm^{-1}) and the lower stratosphere (680.0 cm^{-1}). The channel width of each is 0.625 cm^{-1} . The vertical sensitivity functions of these two channels was computed using the Optimal Spectral Sampling (OSS) method of AER, Inc. for the standard AFGL atmospheric climatology. These sensitivity functions are shown in Figure 6 and indicate that the variation by latitude zone is fairly small.

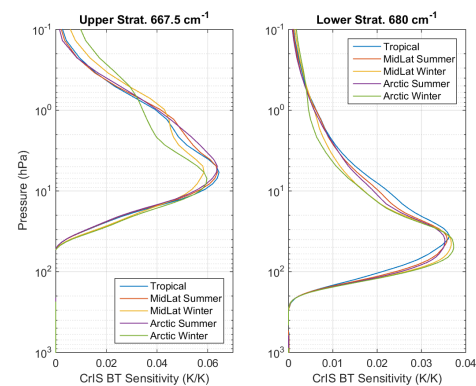


Figure 6. CrIS vertical sensitivity functions for the upper stratosphere (left) and lower stratosphere (right). The colored lines indicate variations in the indicated channel sensitivity due to climatological latitude zone and season.

The daily zonal mean OMPS ozone density profiles were computed using a method very similar to that used in creating the daily mean zonal CrIS brightness temperatures. The OMPS has three near nadir profiles for each scan line. All three profiles were included in the calculation of 10-degree zone mean profiles for each day of the year from April 2012 through March 2016. Since OMPS relies on sunlight as a source, there are no OMPS ozone profiles on the dark side of the Earth.

The CrIS vertical sensitivity functions were used to weight the OMPS ozone density profiles to create a comparison in the upper and lower stratosphere which best represents the CrIS spectral channels. The vertical weights shown in Figure 6 were used based upon the latitude zone which best matched the AFGL climatology.

4. RESULTS

4.1 CrIS BT Inter-annual Variability

The natural variability of the Earth's outgoing infrared emission is illustrated in Figure 7 using three years of CrIS observed brightness temperatures. The carbon dioxide absorption band center is at 667.5 cm^{-1} which has a mean global temperature of about 248 K. Reference to figure 6 shows that the peak sensitivity of this channel (unapodized) is at about 5 hPa which corresponds to an altitude of about 36 km. The CrIS channel at 680.0 cm^{-1} has a global mean brightness temperature of about 220 K and peaks at about 50 hPa or about 22 km. The CrIS dataset used here is limited to three years but it is worth noting that the standard deviation of the stratospheric peaking channels ($650 - 700 \text{ cm}^{-1}$) is less than 0.1 K. This is consistent with results of Brindley et al. (2015) who analyzed five years of IASI brightness temperature spectra. A smaller natural variability leads to shorter trend detection times (Wielicki et al. 2013). Higher variability in the infrared window region ($800 - 1200 \text{ cm}^{-1}$) implies longer detection times in the lower atmosphere.

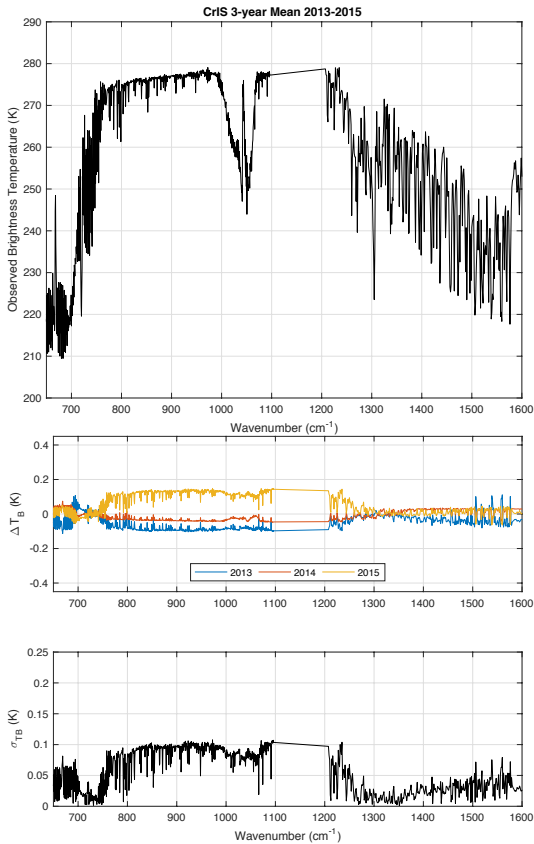


Figure 7. Three-year mean CrIS BT (upper), annual deviation (middle), and inter-annual variability (lower panel).

4.2 OMPS Zonal Mean Profiles

Examples of daily mean ozone density profiles from the OMPS sensor are shown in Figures 8 and 9 for 10-degree latitude zones. The ozone density peaks highest in the equatorial zones. The Northern Hemisphere zones away from the equator show a greater seasonal variation from January to July than do corresponding latitudes in the Southern Hemisphere. The most obvious tendency in the zonal mean profiles is that the ozone density peaks at lower altitudes for high latitudes. Note that the latitudes that are seasonally in darkness have no OMPS profiles.

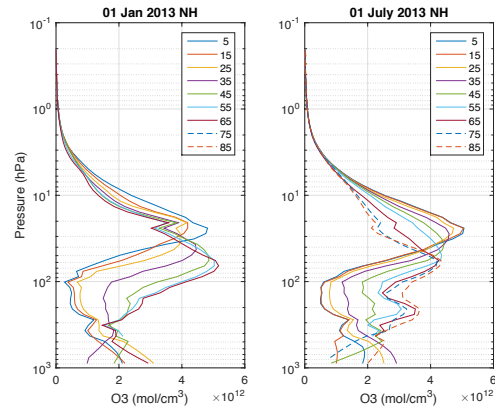


Figure 8. Example daily OMPS ozone zonal mean profiles for January (left) and July (right) 2013 in the Northern Hemisphere.

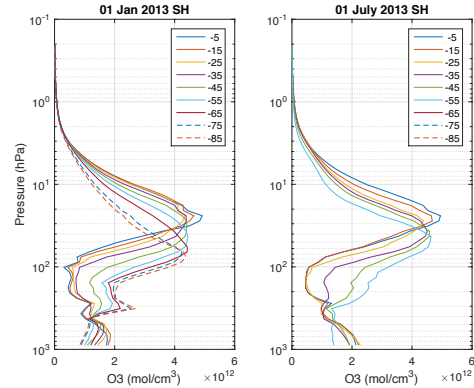


Figure 9. Same as Figure 8 but for the Southern Hemisphere.

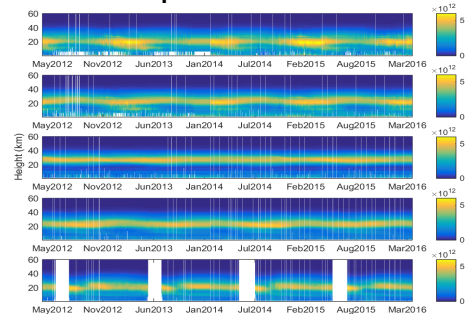


Figure 10. OMPS profiles versus time for latitude zones 65N, 45N, 5N, 45S, and 65S.

4.3 CrIS and OMPS Time Series

Figure 10 illustrates the time series of the OMPS vertical profiles for each day between April 2012 and March 2016 for selected latitude zones. For these same zones the CrIS sensitivity functions were used to compute a weighted average OMPS ozone layer corresponding to the CrIS vertical sensitivity shown in Figure 6. For the upper stratospheric CrIS channel the results are shown in Figure 11. The lower stratospheric time series comparison is shown in Figure 12. The equatorial zone shows relatively constant CrIS brightness temperatures and constant weighted mean OMPS ozone amounts. CrIS BT seasonal variations are apparent in mid-latitudes and largest in the 65N and 65S latitude zones. In the upper stratosphere, the CrIS and OMPS seasonal variations are in phase, however, the CrIS BT seems to lag the OMPS ozone by about six months in the lower stratosphere.

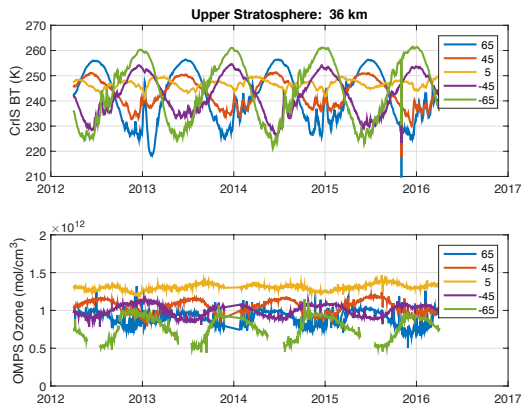


Figure 11. CrIS 667.5 cm⁻¹ upper stratospheric peaking brightness temperature (upper panel) compared with vertically weighted OMPS ozone density profile (lower panel) for the indicated latitude zones.

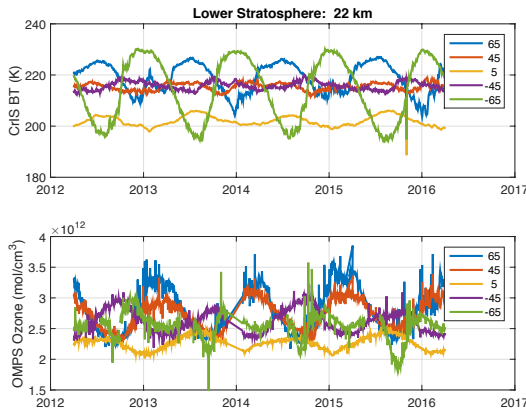


Figure 12. CrIS 680.0 cm⁻¹ lower stratospheric peaking brightness temperature (upper panel) compared with vertically weighted OMPS ozone density profile (lower panel) for the indicated latitude zones.

4.4 CrIS IR BT and OMPS Ozone Correlation

Scatterplots of the time series of daily CrIS and OMPS data are shown in Figures 13 and 14. Table 1 shows the correlation coefficient computed for upper and lower stratosphere and for five latitude zones. In the upper stratosphere there is a larger correlation of CrIS BT with OMPS ozone amount in the extra-tropics. In the lower stratosphere only the 65S zone shows significant correlation between CrIS and OMPS. Short time scale deviations in both BT and Ozone reduce the correlation by increasing scatter.

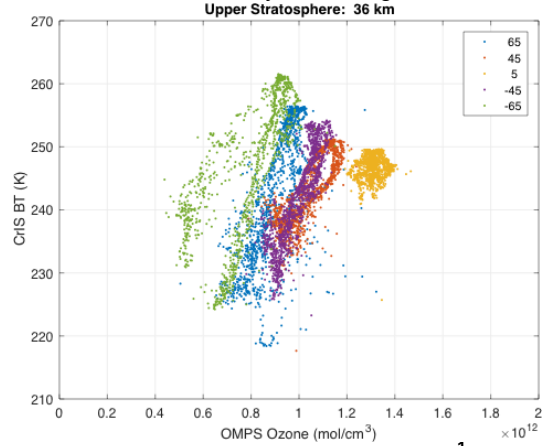


Figure 13. Variations of CrIS 667.5 cm⁻¹ upper stratospheric peaking brightness temperature versus a vertically weighted OMPS ozone density profile for indicated latitude zones.

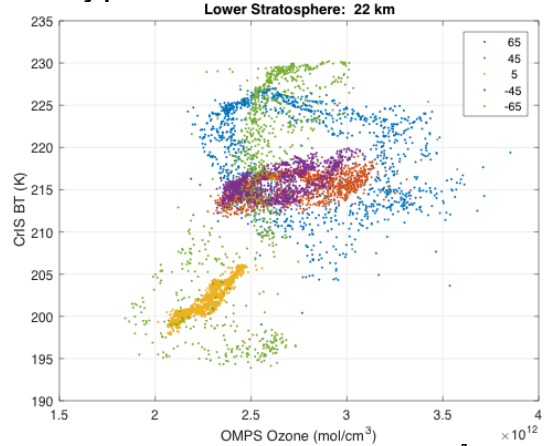


Figure 14. Variations of CrIS 680.0 cm⁻¹ lower stratospheric peaking brightness temperature versus a vertically weighted OMPS ozone density profile for indicated latitude zones.

Table 1. Correlation coefficient between CrIS BT time series and vertically weighted OMPS profile time series.

Zone	65N	45N	5N	45S	65S
Upper Strat.	0.38	0.33	0.006	0.304	0.67
Lower Strat.	-0.20	0.17	0.22	0.16	0.48

5. CONCLUSIONS

An analysis of CrIS nadir brightness temperatures found the inter-annual variability of the infrared channels peaking in the stratosphere to be less than 0.1 K. This result was limited to three calendar years but can be extended as more data become available from Suomi-NPP and the JPSS follow-on satellite platforms. These preliminary results are consistent with previous results from IASI.

A preliminary investigation of the correlation of CrIS infrared brightness temperature variations in the upper and lower stratosphere with OMPS ozone profiles from the same satellite platform has been performed. This study compared CrIS zonal mean brightness temperatures to OMPS zonal mean ozone profiles weighted by the CrIS vertical sensitivity. Seasonal and zonal variations of the CrIS and OMPS observations are most apparent outside the topical zone. In general, the upper stratosphere has higher correlation between infrared brightness temperatures and ozone amount than the lower stratosphere. The exception is the 65S zone of the lower stratosphere where the correlation is comparable. A lag of about six months between infrared brightness temperature and ozone amount is seen in the northern hemisphere lower stratosphere. The complex relationship of IR brightness temperatures and ozone amounts requires further investigation.

Since the OMPS data is limited to sunlit regions, there may be an inconsistency when comparing to the CrIS observations which contain both daytime and nighttime observations. This issue will be addressed in the future by matching the CrIS and OMPS observations in time and space. This matched CrIS/OMPS profile dataset can then be used to compute observations minus calculations. The CrIS 9.6 ozone absorption band will be used for additional validation.

Acknowledgments

The authors acknowledge the support of NASA ROSES grant NNX15AC26G and correspondence with H. Brindley and R. Bantges of Imperial College.

References

Brindley, H., Bantges, R., Russell, J., Murray, J., Dancel, C., Belotti, C. and Harries, J. (2015), Spectral signatures of Earth's climate variability over 5 years from IASI. *Journal of Climate*, 28(4), pp.1649-1660.

Feltz, M. L., Knuteson, R. O., Revercomb, H. E., & Tobin, D. C. (2014), A methodology for the validation of temperature profiles from hyperspectral infrared sounders using GPS radio occultation: Experience with AIRS and COSMIC. *Journal of Geophysical Research: Atmospheres*, 119(3), 1680-1691.

Ho, S.-P., Y.-H. Kuo, W. Schreiner, and X. Zhou (2010), Using SI-traceable Global Positioning System radio occultation measurements for climate monitoring, *Bull. Am. Meteorol. Soc.*, 91(7), S36–S37.

Huang, Y. and V. Ramaswamy (2009), Evolution and trend of the outgoing longwave radiation spectrum. *J. Climate*, 22, 4637-4651, doi:10.1175/2009JCLI2874.1.

Maycock, A. C., 2016: The contribution of ozone to future stratospheric temperature trends, *Geophysical Research Letters*, doi: 10.1002/2016GL068511

Pan, F., X. Huang, L. Strow, and H. Guo, 2015: Linear trends and closures of 10-year observations of AIRS stratospheric channels. *J. Climate*. doi:10.1175/JCLI15-0418.1

Ramaswamy, et al., 2001: Stratospheric temperature trends: Observations and model simulations. *Rev. Geophys.*, 39, 71-122.

Randel, W. J., et al. (2009), An update of observed stratospheric temperature trends, *J. Geophys. Res.*, 114, D02107, doi:10.1029/2008JD010421.

Seidel, D. J., et al., 2016: Stratospheric temperature changes during the satellite era, *J. Geophys. Res. Atmos.*, 121, 664–681, doi:10.1002/2015JD024039.

Steiner, A. K., et al. (2011), GPS radio occultation for climate monitoring and change detection, *Radio Sci.*, 46, RS0D24, doi:10.1029/2010RS004614.

Steiner, A. K., Hunt, D., Ho, S. P., Kirchengast, G., Mannucci, A. J., Scherllin-Pirscher, B., ... & Leroy, S. S. (2013). Quantification of structural uncertainty in climate data records from GPS radio occultation. *Atmospheric Chemistry and Physics*, 13(3), 1469-1484.

Tobin, David, et al. (2013), Suomi-NPP CrIS radiometric calibration uncertainty. *Journal of Geophysical Research: Atmospheres* 118.18.

Wielicki, B., et al., 2013: Achieving Climate Change Absolute Accuracy in Orbit. *BAMS.*, 94, 1519+.